Trap-limited recombination in dye-sensitized nanocrystalline metal oxide electrodes

Jenny Nelson,[1] Saif A. Haque,[2] David R. Klug,[2] and James R. Durrant[2]
[1]*Centre for Electronic Materials and Devices, Department of Physics, Imperial College of Science Technology and Medicine, London SW7 2BZ, United Kingdom*
[2]*Centre for Electronic Materials and Devices, Department of Chemistry, Imperial College of Science Technology and Medicine, London SW7 2AZ, United Kingdom*
(Received 15 May 2000; revised manuscript received 5 January 2001; published 3 May 2001)

We use transient and steady-state optical spectroscopies to study the recombination reaction between electrons and dye cations in a dye-sensitized nanocrystalline TiO_2 electrode in several different chemical environments. Kinetic decay curves are approximately stretched exponential, and the cation half-life, $t_{50\%}$ varies with electron density n as $t_{50\%} \propto n^{-1/\alpha}$, where α is a constant in the range 0.2–0.5. We have developed a model of electron transport in the presence of an energetic distribution of trap states and consider two regimes. In the first, the continuous-time random-walk (CTRW) electrons are free to diffuse through the lattice, by means of multiple trapping events mediated by the conduction band. In the second, the hopping regime, trapped electrons are allowed to tunnel to other, vacant trap sites, or to the dye cation, according to a Miller-Abrahams model for the transition rate. We carry out Monte Carlo simulations of the recombination kinetics as a function of electron density, trap state distributions and other parameters. The CTRW reproduces both the dependence of $t_{50\%}$ on n and the shape of the kinetic curves with only one free fitting parameter, for the case of an exponential density of trap states. The hopping model is ruled out by subnanosecond measurements. We conclude that multiple trapping with a broad energetic distribution of electron traps is responsible for the slow recombination kinetics. When applied to recombination in a nanocrystalline photovoltaic junction at open circuit, the model predicts a sublinear power-law variation of electron density with light intensity G, $n \propto G^{\alpha}$, compatible with the observed behavior.

DOI: 10.1103/PhysRevB.63.205321 PACS number(s): 73.50.Gr, 73.50.Pz, 73.63.−b

INTRODUCTION

A wide range of novel electronic materials, including porous, nanostructured, and molecular solids, are currently being developed for device applications. Porous nanocrystalline metal oxide films are an important example, with applications in photovoltaics,[1] electrochromics,[2] and biosensors.[3] Such films comprise randomly organized nanometer-sized crystallites sintered together into a porous, electronically connected assembly that forms a large-area heterojunction in contact with another medium. The function of devices based on such junctions relies on the mechanisms of charge transport within the film. However, the unusual morphological properties mean that conventional models of charge transport and transfer may not apply. Moreover, dominant charge-transport mechanisms will, in general, be different in the interparticulate and intraparticulate regimes, leading to difficulty in interpreting measurements, such as photocurrent transients, which probe both. Appropriate new experimental probes and theoretical models of the dynamics of charge carriers in such systems are needed.

A configuration of particular interest is the dye-sensitized nanocrystalline photovoltaic cell.[4,5] Visible light is absorbed by a molecular sensitizer adsorbed on the surface of a porous nanocrystalline TiO_2 electrode, and charge separation occurs by rapid electron injection into the TiO_2 while the dye cation is regenerated by a redox active electrolyte. Photoinjected electrons must travel through the porous film to the back contact to complete the circuit. At short circuit this process is apparently very efficient, although slow, and gives rise to a remarkably high internal quantum efficiency.[6] A key question is what happens to the efficiency of electron transport under applied bias, closer to solar cell operating conditions.

It has been established that electron transport in nanocrystalline TiO_2 films is dominated by electron trapping in intraband-gap defect states.[7–11] These are most likely native defects due to oxygen deficiency and adsorbed species at the large film surface area. Transport is traditionally studied by time-resolved and frequency-resolved photocurrent measurements, which probe both interparticulate and intraparticulate electron transport. An alternative is to use transient optical spectroscopy to study the kinetics of the recombination reaction between electrons in the film and adsorbed electron acceptors at the interface. This ''back reaction'' is most important under open-circuit conditions where charge carriers are recycled at the interface and interparticulate transport is at its least important. As is discussed below, by using a redox-inactive electrolyte, this technique can be used to study the back reaction between electrons and photoionized dye molecules. This recombination reaction exhibits a wide range of time scales, which have been attributed to the dynamics of electrons in the TiO_2 crystallites[12–15] probably limited by traps. Though extraordinarily slow under short-circuit conditions, the reaction accelerates under applied bias, apparently due to the increased availability of electrons.[12,13]

In this paper we demonstrate a power-law correlation between the experimentally determined electron density and the observed recombination kinetics for the backreaction. We propose a model for the recombination process show that this behavior results from the capture of electrons in deep traps, and relate our observations to the performance of the solar cell at open circuit. We argue that the simultaneous

observation of electron density and recombination kinetics can be used as a probe of local electron dynamics in other systems.

EXPERIMENT

Nanocrystalline TiO_2 films (average particle diameter 15 nm, >90% anatase) were deposited on F-doped SnO_2-coated glass substrate and sensitized with the dye ruthenium(II) *cis*-(2,2′-bipyridyl-4,4′-dicarboxylate)$_2$(NCS)$_2$ [$RuI_2(NCS)_2$] as previously described.[6] Charge recombination kinetics and electron densities were measured in a three-electrode photoelectrochemical cell as a function of bias applied between a Ag/AgCl reference electrode in the electrolyte and the conducting glass substrate. The applied potential raises the Fermi level in the TiO_2, increasing the electron density. A redox-inactive electrolyte was chosen in order to suppress electron transfer from TiO_2 into electrolyte. Charge recombination was measured by nanosecond-second transient absorption spectroscopy, monitoring the decay of the photoinduced dye cation following excitation by a laser pulse, as described in Refs. 12 and 13. The increase in electron density in the film induced by the applied potential was monitored by measuring the increase in film optical density at 800 nm.[16,17,13] Absolute electron densities were derived from this change in optical absorbance using published values for the extinction cross section per electron in this system at 800 nm.[18–20] Measurements were repeated for two different electrolytes, (a) ethanol containing 0.1*M* tetrabutylammonium triflate and (b) anhydrous acetonitrile containing 0.1*M* lithium perchlorate and 0.1*M* tetrabutylammonium perchlorate. For each electrolyte, the measurements were repeated with different TiO_2 samples.

Charge recombination data are presented in Figs. 1(a) and 1(b). Kinetic curves are approximately stretched exponential (Δ (optical density) $\propto \exp[-t/\tau^{\alpha}]$) with dispersion parameter for (a) $\alpha = 0.3 \pm 0.1$ and for (b) $\alpha = 0.45 \pm 0.1$. Under applied bias, kinetics accelerate with the half-life for re-reduction of the dye cation, $t_{50\%}$, decreasing by about one order of magnitude per 100 mV.[12,13] A bias of -500 to -600 mV corresponds approximately to the operating bias of the solar cell.

As discussed previously,[12,13] the acceleration in the charge recombination process appears to be driven by the increase in the density of electrons in the TiO_2. In principle one should be able to extract the electron density from the applied bias, equating bias shift to a shift in electron quasi-Fermi-level at the film-electrolyte interface. However, this requires knowledge of the density of electron acceptor states in the film, and in particular of intra-band-gap states. Moreover, factors such as resistive losses in the film, electrolyte and contacts, charging of the nanoparticles, and Fermi-level pinning at the interface mean that the relationship between applied bias and Fermi level shift is uncertain.

Instead, we use an experimental technique to monitor electron density. We take advantage of the well-known coloration of the TiO_2 films under applied bias, believed to be due to the filling of Ti 3*d* states, resulting in red-infrared absorbance by electrons in such states. We derive the initial electron density per nanoparticle, *n*, from the measured

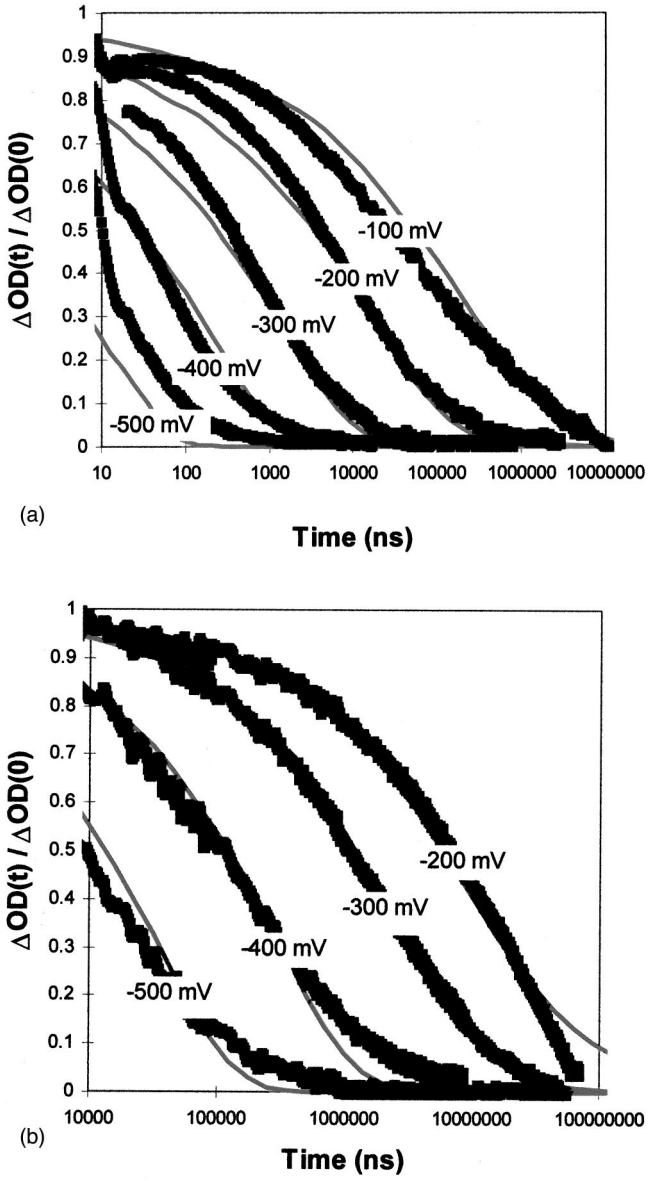

FIG. 1. Charge recombination kinetics for (a) ethanol tetrabutyl ammonium triflate and (b) acetonitrile containing 0.1*M* lithium perchlorate electrolytes as a function of electrical potential applied to the TiO_2 electrode. The dots are experimental data, taken at biases indicated. The solid gray lines are the results of numerical simulations based on the CTRW model, using $\alpha = 0.25$ for (a) and $\alpha = 0.5$ for (b). See text for details.

change in optical density at 800 nm due to the applied bias, ΔOD_{800}, as follows

$$n = \frac{2.303 \Delta OD_{800} \Omega}{\sigma_{ext} d} + n_g , \qquad (1)$$

where σ_{ext} is the electron extinction coefficient at 800 nm, Ω is the volume occupied by a nanoparticle including voids, and *d* the film thickness. The average number of electrons per nanoparticle at positive bias in the dark is much less than 1 and is ignored.[21] n_g is the photogenerated electron density,

which is equal to the number of dye molecules per nanoparticle excited by the laser pulse, assuming 100% efficient injection. σ_{ext} is taken as $4\times10^{-22}\,m^2$ (a decadic extinction coefficient of around 1000 $dm^3\,mol^{-1}\,cm^{-1}$) from the literature.[18,19] The determination of n was calibrated with a second independent measurement, discussed in Ref. 20, where the charge accumulated in the electrode as a function of applied bias was monitored by integrating the transient current drawn in response to a potential step. Comparison of the bias-dependent accumulated charge with the change in optical density implies a value of σ_{ext} which agrees with the published values. Ω is taken to be $8\times10^{-24}\,m^3$ (1×10^{14} nanoparticles in a film of volume $8\times10^{-10}\,m^3$) and the film thickness as 8 μm in all cases, as measured. We let $n_g=1$, given that light intensities are such that, on average, one dye is excited per nanoparticle. The combined effect of the uncertainties in the factors used in Eq. (1) is a systematic error of up to a factor of 2 in converting optical density to n. The error in the measured absorbance is less than 5%.

In Figs. 2(a) and 2(b) the $t_{50\%}$ values obtained from the data shown in Fig. 1 are plotted against the initial electron densities per nanoparticle, at the same biases. Additional data points are taken from Ref. 13. The data indicate clearly that the relationship between $t_{50\%}$ and n is a power-law form,

$$t_{50\%} \propto n^{-1/\alpha} \tag{2}$$

with $\alpha=0.25\pm0.05$ for Fig. 2(a) and $\alpha=0.46\pm0.05$ for Fig. 2(b). The same value of α was obtained, within the errors, for different repeats of the same experiment, showing that the value of α is not due to the particular TiO_2 sample used. Notice that in the bias range studied the electron density is in the range of 1 to 100 s of electrons per nanoparticle. The power-law behavior is insensitive to uncertainties in the factors used to derive n, with a change in σ_{ext} of a factor of 2 changing the values of α only slightly [by ±0.01 for Fig. 2(a) and ±0.05 for Fig. 2(b)]. Such behavior has never previously been reported for dye-sensitized systems. The observation by others[19,22] of a power-law dependence of recombination kinetics on electron density refers to the dark recombination reaction between electrons and I_3^-. This reaction is in principle different, although the origin of the power-law behavior may be related and is discussed below. The values of α obtained from these plots agree within errors with the values of α obtained from stretched exponential fits to the decay kinetics shown in Fig. 1. This behavior is expected for a diffusion-limited recombination process, as discussed below.

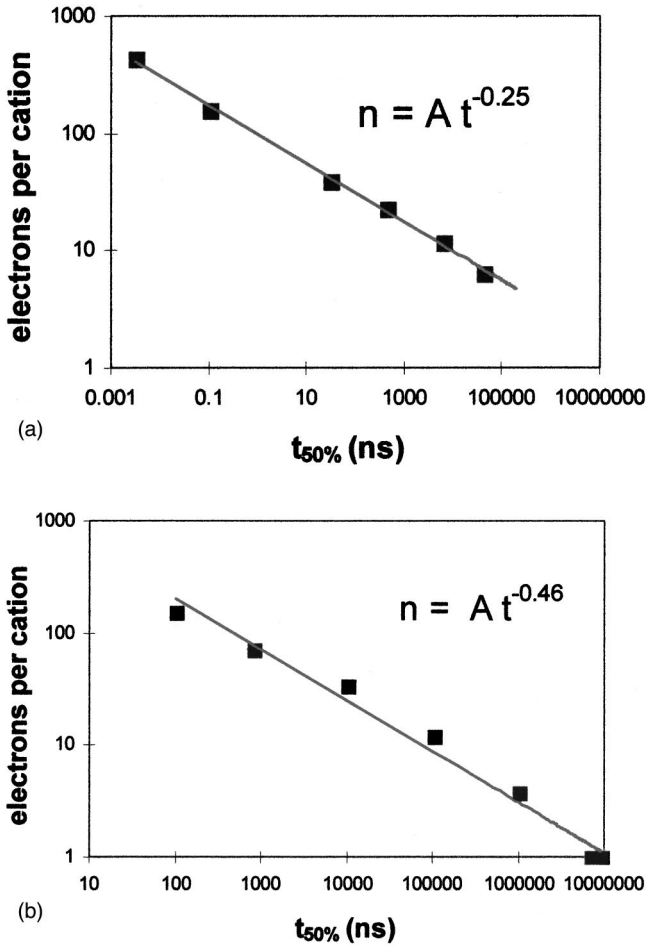

FIG. 2. Double-logarithmic plots of the initial number of electrons per nanoparticle after excitation by laser pulse against the time $t_{50\%}$ at which the cation density decays to half of its original value for (a) ethanol tetrabutyl ammonium triflate and (b) acetonitrile containing lithium perchlorate. The straight lines are best fits to the data. The uncertainty in $t_{50\%}$ is indicated by the width of the filled squares.

MODELS

To find a quantitative explanation for the observed behavior we consider the kinetics of the bimolecular reaction $n+S\rightarrow0$ between a population of n mobile walkers (electrons) and S stationary targets (cations). Second-order reaction kinetics predict that $S(t)$ evolves with time t according to

$$\frac{dS}{dt}=-BSn, \tag{3}$$

where B is a constant. In the limit where $n\gg S(0)$, $S(t)$ varies like e^{-Bnt} and $t_{50\%}$ varies like n^{-1}, in clear disagreement with our observations. The model of Eq. (3) is equivalent to the situation where a random distribution of electrons is free to diffuse normally in the presence of a number of dye cations, with recombination occurring whenever an electron and a dye cation meet.

To explain the range of time constants which is observed experimentally we need to introduce some degree of disorder. We do this through an energetic and spatial distribution of electron trap states. The nanoparticle is modeled as a sphere or a spherical shell containing a regular cubic lattice of electron acceptor sites. Some fraction ϕ of these sites are traps with energies E drawn from a distribution function $g(E)$; the remainder are conduction-band sites with energy E_c. Initially n sites are populated with electrons and one site is occupied by a dye cation. For consistency with Fermi

Dirac statistics each site can be occupied only once. Recombination occurs whenever an electron arrives on a site occupied by the dye cation.

We distinguish two regimes. In the first, the diffusion-limited regime, electrons experience no long-range forces but are free to wander throughout the lattice, moving to a nearest neighbor after an interval, called the *waiting time*, which depends upon the activation energy of the site currently occupied. This is a modification of Fickian diffusion known as a continuous-time random walk (CTRW).[23–27] In the second, the tunneling limited (hopping) regime, electrons are normally immobilized in traps but experience long-range interactions from dye cations and vacant sites that allow rare tunneling events from site to site.

Multiple trapping limited recombination (CTRW)

In the simplest form of the CTRW, steps to all nearest neighbors are equally likely and the waiting time depends only upon the energy of the initial site. This is essentially a model of electron transport mediated by the conduction band or multiple trapping. Physically, it is a model of thermally activated electron transfer in a strongly screened environment. In the case of the nanocrystalline electrode, strong screening of electrons results from the high dielectric constant and interpenetrating electrolyte.[28,29] Apart from the density of trap states and nanoparticle geometry, the only parameter required is the time for the fastest electron hop $t_{\min}$. This need not be identical to the thermal hopping time (although that value provides a lower limit) since the absolute time scale cannot be distinguished from the fraction of sites that are traps.

We are encouraged to use the CTRW for the following reasons. In the CTRW, the time for each step is taken from a waiting time distribution $\chi(t)$. Consider the case of an exponential density of trap states, $g(E)$:

$$g(E)=\frac{\alpha N_t}{kT}e^{-\alpha(E_c-E)/kT}, \tag{4}$$

where E_c is the conduction-band edge energy, N_t is the density of traps per unit volume (such that $\phi=N_t a^3$ where a is the lattice constant), k is Boltzmann's constant, T is the temperature, and α is the dispersion parameter such that $0<\alpha<1$. For this distribution $\chi(t)$ has the power-law form

$$\chi(t)\propto t^{-1-\alpha}. \tag{5}$$

Now, for a waiting-time distribution with a sufficiently long tail the *average number of steps taken by any walker in time t*, $H(t)$, increases more slowly than t. In the particular case of the power law $\chi(t)$,[30]

$$H(t)\propto t^{\alpha}. \tag{6}$$

This behavior of $H(t)$ determines the kinetics of the bimolecular reaction $n+S\rightarrow 0$. For mobile walkers and stationary targets the rate determining step is the time taken for a walker to reach a target (the *first passage time*). In the limit where the lattice is sparsely occupied and walkers outnumber targets ($n\gg S$) the target survival probability varies as[31]

$$S(t)=S(o)e^{-BnH(t)}, \tag{7}$$

where n is the density of walkers and B is a constant. The half-life $t_{50\%}$ of the targets, defined by $S(t_{50\%})=\frac{1}{2}S(o)$, is given in the case of a general $H(t)$ by

$$t_{50\%}=H^{-1}\left(\frac{\ln 2}{Bn}\right), \tag{8}$$

where H^{-1} is the inverse function of H. In the special case of the power law $\chi(t)$, which corresponds to an exponential density of states, $S(t)$ is a stretched exponential

$$S(t)\propto e^{-(t/\tau)^{\alpha}} \tag{9}$$

and $t_{50\%}\propto n^{-1/\alpha}$ [Eq. (2)] exactly as observed above. This is in marked contrast with the behavior $t_{50\%}\propto n^{-1}$, which is expected for homogeneous second-order reaction kinetics and for a normal random walk where $H(t)\propto t$. Thus, at least for the case of an exponential distribution of trap states, the CTRW provides an explanation for both the remarkable power-law dependence of $t_{50\%}$ on n and the stretched exponential kinetic behavior.

Tunneling-limited recombination (hopping model)

In the hopping model a trapped electron can reduce the dye cation by quantum-mechanical tunneling to the dye site.[32] For weak electron-cation interactions, the electron transfer rate k_{ET} is governed by Fermi's golden rule and is expected to vary as the square of the overlap of electron and dye wave functions. We model the electron transfer rate k_{ET} by

$$k_{\mathrm{ET}}=k_S e^{-r_{iS}/a_B}, \tag{10}$$

where k_S is a constant representing the strength of the electron-cation interaction, r_{iS} is the electron-cation separation, and a_B is the effective Bohr radius. The extent of the cation wave function is known to be short compared to the TiO_2 lattice constant because of the relatively high electron affinity of the cation, and therefore the dominant contribution to a_B is from the electron wave function. a_B is assumed to depend on the trap energy E_i through

$$a_B(E_i)=a_0/\sqrt{E_C-E_i}, \tag{11}$$

where a_0 is a constant. Now, since an electron may be stabilized in any vacant trap, an electron at site i with a Bohr radius of $a_B(E_i)$ is also capable of hopping to vacant electron acceptor sites j. For the corresponding transfer rate we invoke the Miller-Abrahams model[33,34]

$$k_{ij}=k_0 e^{-r_{ij}/a_B(E_i+E_{ij})}e^{-E_{ij}/kT}, \tag{12}$$

where k_0 is a constant representing the strength of the electron–vacant-site interaction, r_{ij} is the separation of initial and final site, and

$$E_{ij}=\begin{cases} E_j-E_i & \text{if } E_j>E_i \\ 0 & \text{otherwise} \end{cases} \tag{13}$$

represents the activation energy required to step *up* to a higher energy site. The argument of a_B ensures that the higher of the two energies E_i and E_j is used, that is, tunneling is thermally assisted. The difference in rate constants k_S and k_0 allows for differences in the Frank-Condon factors for the two types of transition. Physically, this model should apply where the release time from deep traps is long compared to $1/k_S$. In this case we define, for purposes of comparison, $t_{\min}$ as the mean time for an electron at the Fermi level in equilibrium to hop to a nearest neighbor of equal or lower energy,

$$t_{\min}=\frac{e^{a/a_B(E_F)}}{k_0}. \tag{14}$$

RESULTS

For each model we carry out Monte Carlo simulations of the transport of electrons within a nanoparticle in the presence of a dye cation. The standard case nanoparticle has radius 17 units, representing a 7-nm radius[35] and a lattice constant of 0.4 nm.[36] Electrons may be constrained to occupy only sites within a few atomic layers of the surface of the nanoparticle (''shell'') or the entire volume (''sphere''). In all cases we use an exponential distribution of trap states (3) with α as a parameter. At the start of each simulation, n lattice sites are occupied at random by electrons. In the CTRW, every time an electron moves into a new site it adopts a waiting time given by

$$(\ln X)t_{\min}e^{(E_C-E)/kT}, \tag{15}$$

where E is the energy of the site currently occupied and X is a random number between 0 and 1. At every step, the electron with the shortest waiting time moves to one of its neighbors at random, and the waiting times of the remaining electrons are advanced by that interval, as described in Ref. 15. Electrons implanted at random quickly relax into traps. When an electron walks to the site occupied by the dye cation, the time is recorded and the simulation stops. The relationship between the rate of electron emission from an occupied trap, given by $t_{\min}^{-1}e^{-(E_C-E)/kT}$, and the rate of capture of a conduction-band electron by a vacant trap, $t_{\min}^{-1}$, together with the condition of single occupancy of trap sites ensures that the electronic energies obey Fermi Dirac statistics. Inspection of the energies of a relaxed electron population confirms that the Fermi Dirac distribution is reproduced.

In the case of the hopping model, the electrons are initially implanted into trap sites. The i^{th} electron adopts a waiting time that is the shortest of the hopping times to each of the other vacant traps in the lattice, given by

$$(\ln X)k_0^{-1}e^{r_{ij}/a_B}e^{E_{ij}/kT}, \tag{16a}$$

and to the dye, given by

$$(\ln X)k_S^{-1}e^{r_{is}/a_B}. \tag{16b}$$

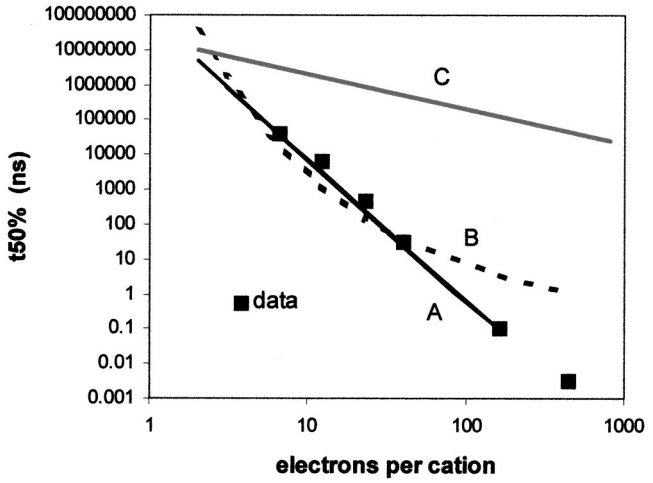

FIG. 3. Comparison of experimental results for n vs. $t50\%$ for the ethanol electrolyte (filled squares), with results of the CTRW model with $\alpha=0.25$ (curve *A*) and the hopping model in the limit where $k_S \gg k_0$ (curve *B*). Notice that over narrow ranges of $t_{50\%}$ the hopping model appears to resemble the data and can only be ruled out by the subnanosecond data, which is capable of distinguishing between the models. Curve *C* shows the variation expected for normal diffusion when $n \propto t_{50\%}^{-1}$. The recombination times predicted in that case are clearly incompatible with the data.

It is assigned a destination that is the site j with the shortest hopping time or the dye, whichever has the shorter time. (To save computational effort transitions to conduction-band states are not considered since these are extremely unlikely.) Then, the electron with the shortest waiting time moves to its destination, its waiting time is recalculated for its new location, and the waiting times of all other electrons are advanced. Again, once an electron arrives on the site of the dye cation the simulation stops. Cation lifetime distributions are compiled from 5000 simulations and the procedure repeated for the range of electron densities in Fig. 2 and variations in other parameters. The parameter

$$\gamma=-d(\log n)/d(\log t_{50\%}) \tag{17}$$

is evaluated from the results.

For the CTRW we use values of α consistent with the observed values in Fig. 2 and treat $t_{\min}$ as a fitting parameter. In the case of the acetonitrile electrolyte where it is not always true that $n \gg S$, the observed value of α is expected to be smaller than the theoretical value.[37] In this case we use for α a value of 0.50, slightly larger than the observed exponent of 0.46. In the case of the ethanol electrolyte where $n \gg S$, we use $\alpha=0.25$, as observed. Best fits are obtained with $t_{\min}=2\times10^{-15}$ s for the ethanol electrolyte and 2.5×10^{-9} s for the acetonitrile electrolyte, when the fraction of traps ϕ is 1. Simulated $S(t)$ are compared with experimental curves in Fig. 1, showing that both the shape of the kinetic curves and the n dependence is reproduced.

In Fig. 3, simulated and measured n vs $t_{50\%}$ are presented for the ethanol system, confirming the power-law behavior predicted by the model. The n vs. $t_{50\%}$ behavior expected for

TABLE I. Value of $\gamma = -d(\log n)/d(\log t_{50\%})$ for n in the range $1 < n < 150$ from simulations using the hopping model. Strongly dispersive behavior results only for cases where the electron-cation interaction is very strong or the fraction of trap sites is small, i.e., where tunneling to the dye cation is greatly preferred to tunneling between trap sites. (Results for $a_0 > 1$ do not differ substantially for $a_0 = 1$ and are omitted.)

α	Sphere or shell	a_0	ϕ	k_S/k_0	γ
0.25	Sphere	0.5	0.1	1	1.00
0.25	Shell	1	0.1	1	1.00
0.25	Shell	0.2	0.1	1	0.86
0.5	Shell	0.5	0.1	1	0.96
0.75	Shell	0.5	0.1	1	0.96
0.25	Shell	0.5	0.01	1	0.63
0.25	Shell	0.5	0.1	1000	0.45
0.25	Shell	0.5	0.01	1000	0.37

simple diffusion, as expected from Eq. (3), is presented for comparison. Clearly, the CTRW model is consistent with our observations while simple diffusion is not.

Notice that in the CTRW, kinetics are dominated by the energetic distribution of trap states rather than the geometry. Variations in ϕ and in the geometry of the nanoparticle (shell or sphere) do not affect the n vs $t_{50\%}$ behavior but merely increase or decrease the $t_{\min}$ needed for best fit.

In the case of the hopping model we use α, ϕ, k_S/k_0, and a_0 as parameters and seek some combination that gives rise to the strong sensitivity of $t_{50\%}$ to n that is observed. We consider the effect of varying each of these parameters within the range of values that is physically reasonable for our system. k_S/k_0 is varied between 1 and 1000. a_0 is varied between 0.2 and 5 lattice units $eV^{1/2}$, spanning the range between the value quoted for the Bohr radius of a conduction-band electron in rutile[38] and an upper limit estimate for the Bohr radius in anatase.[38] ϕ is varied between 1 and 0.01 for both sphere and shell geometries, varying the number of trap states per nanoparticle from thousands to a few tens. α is varied between 0 and 1. Illustrative results for γ are summarized in Table I.

It is clear that in this case kinetics are dominated by the *spatial* rather than the *energetic* distribution of trap states. For the default case parameters, the sensitivity of $t_{50\%}$ to n that is observed for either system cannot be reproduced by the hopping model. Instead, values of γ rather close to 1 are obtained irrespective of the breadth of the trap distribution (α). Strong sensitivity of $t_{50\%}$ to n can only be obtained by making $k_S \gg k_0$ and reducing the number of traps. In this limit, electron hopping directly to the cation is much more likely than hopping to another vacant site. This widens the spread of hop distances and hence range of time constants. For some parameter combinations in this limit, values of γ similar to those observed can be obtained for n in the range 1–100. However, because the recombination occurs after a very small number of hops, the model fits the data only if very small values are used for k_0, leading to long times ($> \mu$s) for the nearest-neighbor hopping time $t_{\min}$. Such time scales for hopping are physically implausible, and are not

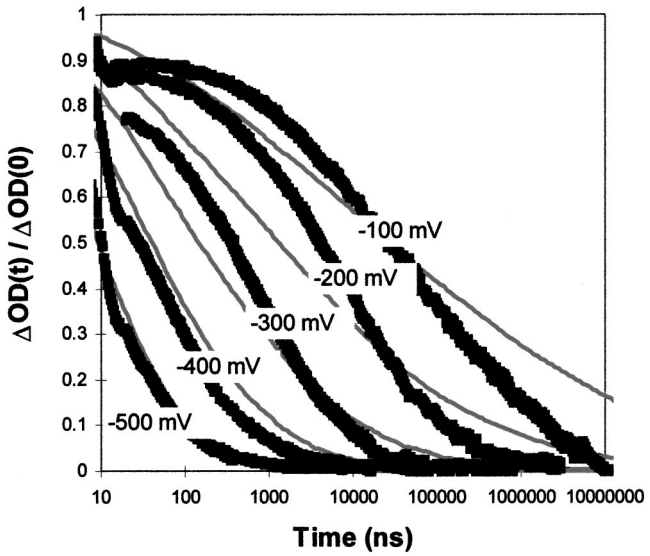

FIG. 4. Simulations using the hopping model in the limit where $k_S \gg k_0$ in comparison with the data set for the ethanol electrolyte. The comparison shows that although the observed $t_{50\%}$ values can be fitted approximately by the hopping model, the shape of the curves is not reproduced.

consistent with multiphasic behavior on nanosecond time scales observed in for the ethanol electrolyte.

To illustrate the point, we consider the limit where $k_0 \rightarrow 0$ and traps are isoenergetic. In this limit, the problem can be simplified to one of competition between immobilized electrons for the cation. The cation density evolves approximately as

$$\frac{dS}{dt} = S_0 \sum_i \exp[-k(e^{\mathbf{r}_{is}/a_B})t], \tag{18}$$

where $\mathbf{r}_{is}$ is the separation between the ith electron and the dye cation. Simulated $t_{50\%}$ vs n values are presented in Fig. 3 and recombination kinetics in Fig. 4. It is clear that although $\log t_{50\%}$ vs $\log n$ is approximately linear over a limited range of n, at very fast (subnanosecond) times the simulation diverges from the data, while the CTRW model does not. Moreover, the recombination kinetics do not resemble stretched exponentials and do not fit the data well, as shown in Fig. 4. Thus we conclude, on the basis of our subnanosecond observations, that the hopping model on its own does not explain the data.

We would like to comment on the rather surprising different behavior of the two models in the other limit, where the number of trap states is large. For short a_B, the hopping model approaches a nearest-neighbor hopping variant of the CTRW, where the time for an electron hop to a nearest neighbor is determined by the increase in energy between initial and final states. It has previously been shown that the asymptotic form of the waiting time distribution for this variant approaches that of the simple multiple-trapping CTRW,[39] leading to similar asymptotic kinetics in simulated photocurrent transients.[40] The different behavior for *recombination*

kinetics, when electron and ''hole'' populations are asymmetric, is due to the fact that recombination samples only the *fastest* electron hops. The dye cation will be reduced by the first electron to arrive at the dye site, and electrons that are trapped for a long time are irrelevant. In this short time range, the waiting times sampled are those for the easiest hops and the asymptotic waiting time distribution is not reached. In the case of the multiple trapping CTRW slow events *must* be sampled because the electron that reduces the cation must, at some point in its trajectory, escape from deep traps.

DISCUSSION

From the above results it is clear that multiple trapping of electrons on a energetic distribution of trap states is capable of explaining the observed recombination kinetics while a model based on electron tunneling alone is not.

Multiple trapping has been invoked to explain other dynamic phenomena in nanocrystalline TiO_2 electrodes such as frequency dispersion in intensity-modulated photocurrent/photovoltage spectroscopy[11,19,41] and dispersive photocurrent transients.[8] The advantages of the present approach are that our technique probes electron dynamics on the intraparticulate scale and is not influenced by electron transport across grain boundaries between nanoparticles, and that changes in quasi-Fermi-level in the course of the experiment are relatively small.

We should comment on the nature of the trapped electrons and the form of the density of trap states. In both anatase and rutile TiO_2 intra-band-gap Ti(III) states result from the localization of an electron in the Ti $3d$ orbital in the presence of an electron donating defect.[42] These defect-induced states are observed to lie 2–3 eV above the valence-band maximum and act as electron traps. Although oxygen vacancies are the best studied defects, surface binding and intercalation of cations[43,44] and proton insertion[45] also lead to the formation of Ti(III) states. In our systems, adsorbed species and nonstoichiometry at the large and disordered surface of the nanocrystalline TiO_2 electrode are expected to lead to a range of defect states, extending over a range of energies into the band gap. The quantitative differences in the exponent α for the different electrolytes indicate that the *electrolyte* influences the density of trap states. We attribute this to differences in the nature and density of localized states resulting from the intercalation or surface binding of Li^+ ions (in the case of the acetonitrile electrolyte) and proton insertion (in the case of the weakly acidic ethanol electrolyte).

There is some debate about whether the species responsible for the visible absorption in biased TiO_2 electrodes are conduction-band or trapped electrons.[16,46] This distinction is rather blurred as the conduction in TiO_2 is generally believed to be by small polaron hopping with the electron moving between Ti $3d$ states that are relatively localized on Ti ions, while ''trap'' states are similar in nature but more strongly localized. We believe that the electrons we observe are trapped in defect states, because the range of time constants points to a spread in activation energies that would not result for small polaron hopping in a perfect crystal. In any case it is clear that the electrons in TiO_2 are *functionally* trapped.

The choice of an *exponential* density of states is arbitrary. However, (i) we have bias-dependent capacitance studies that indicate an exponential increase in stored charge with bias,[20] (ii) it has been shown previously[47] that similar dispersive transport behavior results from a small number of discrete trap energies as from exponentials, and (iii) the factor that influences CTRW kinetics is the shape of the density of states over the range of electron Fermi levels sampled during the simulation, i.e., those states close to the Fermi level that are which are most likely to be occupied or emptied. When the electron density is a small fraction of the density of available trap states this means the tail of the distribution. This is likely to be approximated by an exponential even when the density of states closer to the conduction-band edge has different structure.

Despite the success of the CTRW in modeling the observed recombination kinetics it is not possible to rule out some dependence of observed recombination kinetics on the dye-cation recombination step. This step is also likely to determine the absolute time scale of the recombination process through k_S. Such a dependence is beyond the scope of this paper.

Multiphasic kinetics are commonly found in disordered systems, and many examples of stretched exponential decays have been reported.[48] These have been attributed variously to hopping or thermal activation of carriers between a distribution of trap states and to the geometry of the underlying structure. A stretched exponential decay by no means specifies the carrier dynamics uniquely. Here by studying the correlation of recombination kinetics with electron density we have provided evidence for thermal activation out of trap states as the cause of stretched exponential kinetics in this case. The principle and the techniques should be applicable to other porous and heterogeneous electronic materials.

Relevance for the solar cell

In the solar cell the most important recombination reaction is reduction of the oxidized species or *holes* in the electrolyte—usually I_3^-—by electrons in TiO_2. Now if we suppose that the hole moves slowly compared to the electron so that it is more or less fixed at a surface site and that the first encounter between electron and hole is the rate-limiting step, the rate of disappearance of electrons *per hop* can be written

$$\frac{dn}{dH} = -A_r p n, \tag{19}$$

where p is the concentration of holes and A_r is a constant. Under constant illumination electrons are generated at a rate G per unit time and volume, so that one new electron is introduced into a nanoparticle every τ_g seconds where $\tau_g = 1/\Omega G$. Now since the number of hops in time τ_g varies as $(\tau_g)^{\alpha}$,[30] the rate of electrons generated per hop is propor-

tional to $\tau_g^{-\alpha}$ and hence to G^{α}. Consider the situation at open circuit. If diffusive currents are small (i.e., internal fields are negligible and generation uniform) then recombination balances generation at every point and, balancing the rates per hop,

$$\frac{dn}{dH} = A_g G^{\alpha} - A_r p n = 0, \tag{20}$$

whence

$$n \propto G^{\alpha}, \tag{21}$$

Electron density thus decreases sublinearly with light intensity. Such behavior has been observed in the frequency domain by Schlichthorl, Park, and Frank, who report $n \propto G^{0.45}$ (Ref. 22) and Franco *et al.*, who report $n \propto G^{0.6}$ (Ref. 19). Indeed such behavior is believed to be responsible for the good performance of the solar cell at low light intensities. Elsewhere[49] this behavior has been explained in terms of a recombination reaction between the electron and tri-iodide which is second order in n. Ours is an alternative explanation which is compatible with first-order recombination: trapping alone *could* lead to the observed recombination behavior at low intensities.[50] To a first approximation we do not expect trapping to influence the dependence of the open-circuit voltage V_{OC} on light intensity: it is straightforward to show from Eq. (20) and an exponential density of states that $\Delta V_{OC} \propto kT \ln G$, assuming that V_{OC} is controlled only by the electron Fermi level.

As a further note in support of multiple trapping, we point out that the model leads to a density of conduction-band electrons, n_c, that varies with the total electron density like $n_c \propto n^{1/\alpha}$. This is again consistent with Ref. 22, which reports $n_c \propto n^{2.7}$.

CONCLUSION

In conclusion, we have studied the recombination reaction between electrons and dye cations in dye-sensitized TiO_2 electrodes in different redox inactive environments. We find that the kinetic decay curves are approximately stretched exponential and the cation half-life $t_{50\%}$ varies with electron density n like as $t_{50\%} \propto n^{-1/\alpha}$, where α is a constant in the range 0.2–0.5. The wide range of observed time constants and high sensitivity of kinetics to electron density cannot be explained by homogeneous second-order reaction kinetics, which predict that $t_{50\%} \propto n^{-1}$, but can be explained by a continuous-time random-walk model of electron transport in the presence of an energetic distribution of trap states. We have shown that this model, in which electrons diffuse through the lattice undergoing multiple trapping events in intra-band-gap trap states, leads to the observed dependence of $t_{50\%} \propto n^{-1/\alpha}$ for an exponential distribution of states, thus explaining the strong dependence of kinetics upon applied electrical bias. It also reproduces the temporal shape of the kinetic curves with only one free-fitting parameter. In a second model, where electrons are essentially immobilized in traps on the time scale of the experiment but are allowed to undergo tunneling events to other, vacant trap sites or to the dye cation observed kinetics can only be reproduced in the limit where electron-cation transitions dominate, and then only for slower (>nanosecond) measurements. However some influence of the dye-cation recombination step on observed recombination kinetics cannot be ruled out.

We conclude that electron trapping is responsible for the observed recombination kinetics and that the distribution of trap states is likely to be critical. When the same model is applied to the recombination reaction between electrons and oxidized species in the electrolyte (which is the primary reaction determining the voltage output of the solar cell) in a nanocrystalline junction at open circuit, the model predicts a sublinear power-law variation of electron density with light intensity G, $n \propto G^{\alpha}$. This has been observed by other authors but has not previously been explained in terms of electron transport. The optical measurement of recombination kinetics between conduction electrons and surface adsorbed species is sensitive to local electron dynamics can be used more generally as a probe of electron transport in other porous materials or heterogeneous systems.

ACKNOWLEDGMENTS

This work was supported by the Engineering and Physical Sciences Research Council and the Greenpeace Environmental Trust. We are grateful to Carol Olson, Richard Willis, and Yasuhiro Tachibana for helpful discussions.

[1] M. Grätzel, Curr. Opin. Colloid Interface Sci. **4**, 314 (1999).
[2] C. Bechinger, S. Ferrere, A. Zaban, J. Sprague, and B. A. Gregg, Nature (London) **383**, 608 (1996).
[3] E. Topoglidis, A. E. G. Cass, G. Gilardi, S. Sadeghi, N. Beaumont, and J. R. Durrant, Anal. Chem. **70**, 5111 (1998).
[4] B. O'Regan and M. Grätzel, Nature (London) **353**, 737 (1991).
[5] A. Hagfeldt and M. Grätzel, Chem. Rev. **95**, 49 (1995).
[6] M. K. Nazeeruddin, A. Kay, I. Rodicio, R. Humphry-Baker, E. Muller, P. Liska, N. Vlachopoulos, and M. Grätzel, J. Am. Chem. Soc. **15**, 6382 (1993).
[7] K. Schwarzburg and F. Willig, Appl. Phys. Lett. **58**, 2520 (1991).
[8] R. Konenkamp, R. Henninger, and P. Hoyer, J. Phys. Chem. **97**, 7328 (1993); also R. Konenkamp and R. Henninger, Appl. Phys. A: Solids Surf. **58**, 87 (1994).
[9] A. Hagfeldt, S.-E. Lindquist, and M. Grätzel, Sol. Energy Mater. Sol. Cells **32**, 245 (1994).
[10] F. Cao, G. Oskam, G. J. Meyer, and P. C. Searson, J. Phys. Chem. **100**, 17 021 (1996).
[11] P. E. de Jongh and D. Vanmaekelbergh, Phys. Rev. Lett. **77**, 3427 (1996).
[12] S. A. Haque, Y. Tachibana, D. R. Klug, and J. R. Durrant, J. Phys. Chem. B **102**, 1745 (1998).
[13] S. A. Haque, Y. Tachibana, R. L. Willis, J. E. Moser, M. Grätzel, D. R. Klug, and J. R. Durrant, J. Phys. Chem. B **104**, 538

(2000).
[14] G. M. Hasselmann and G. J. Meyer, J. Phys. Chem. B **103**, 7671 (1999).
[15] J. Nelson, Phys. Rev. B **59**, 15 374 (1999).
[16] G. Rothenberger, D. Fitzmaurice, and M. Grätzel, J. Phys. Chem. **96**, 5983 (1992).
[17] B. O'Regan, M. Grätzel, and D. Fitzmaurice, J. Phys. Chem. **95**, 10 525 (1991).
[18] U. Kolle, J. Moser, and M. Grätzel, Inorg. Chem. **24**, 2253 (1985).
[19] G. Franco, J. Gehring, L. M. Peter, E. A. Ponomarev, and I. Uhlendorf, J. Phys. Chem. B **103**, 692 (1999).
[20] C. Olson, R. L. Willis, J. Nelson, and J. R. Durrant (unpublished).
[21] As reported in Ref. 13, absorbance in the dark at biases more positive than 0 mV for the ethanol electrolyte and −100 mV for the acetonitrile electrolyte (b) is smaller than the sensitivity of our spectrometer (which corresponds to an electron density of less than 0.5 electrons per nanoparticle as calculated in the text) and insensitive to bias. This indicates the electron density in the dark is less than 0.5.
[22] G. Schlichthorl, N. G. Park, and A. J. Frank, J. Phys. Chem. B **103**, 782 (1999).
[23] H. Scher and E. W. Montroll, Phys. Rev. B **12**, 2455 (1975).
[24] M. Silver and L. Cohen, Phys. Rev. B **15**, 3276 (1977).
[25] T. Tiedje and A. Rose, Solid State Commun. **37**, 49 (1980).
[26] A. Blumen and G. Zumofen, J. Phys. Chem. **77**, 5127 (1982).
[27] M. A. Tamor, Phys. Rev. B **36**, 2879 (1987).
[28] B. A. Gregg, A. Zaban, and S. Ferrere, Z. Phys. Chem. (Munich) **212**, 11 (1999).
[29] D. Cahen, G. Hodes, M. Grätzel, J. F. Guillemoles, and I. Riess, J. Phys. Chem. B **104**, 2053 (2000).
[30] A. Blumen, J. Klafter, and G. Zumofen, in *Optical Spectroscopy of Glasses*, edited by I. Zschokke (Reidel, Dordrecht, 1986).
[31] A. Blumen, G. Zumofen, and J. Klafter, Phys. Rev. B **30**, 5379 (1984).
[32] W. Schmickler, *Interfacial Electrochemistry* (Oxford University Press, Oxford, 1996).
[33] A. Miller and E. Abrahams, Phys. Rev. **120**, 745 (1960).
[34] H. Bässler, Phys. Status Solidi B **175**, 15 (1993).
[35] C. J. Barbe, F. Arendse, P. Compte, M. Jirousek, F. Lenzmann, V. Shklover, and M. Grätzel, J. Am. Ceram. Soc. **80**, 3157 (1997).
[36] Ti-Ti distances in anatase are 3.79 and 3.04 Å. [See, e.g., R. Sanjines, H. Tang, H. Berger, F. Gozzo, G. Margaritondo, and F. Levy, J. Appl. Phys. **75**, 2945 (1994).]
[37] Test simulations show that for an exponential $g(E)$, $t_{50\%} \propto n^{-1/\alpha}$ in the limit where $n \gg S$, as originally expected
[38] H. Tang, K. Prasas, R. Sanjines, P. E. Schmid, and F. Levy, J. Appl. Phys. **75**, 2042 (1994).
[39] B. Hartenstein, H. Bassler, A. Jakobs, and K. W. Kehr, Phys. Rev. B **54**, 8574 (1996).
[40] M. Silver, G. Schönherr, and H. Bässler, Phys. Rev. Lett. **48**, 352 (1982).
[41] D. Vanmaekelbergh and P. E. de Jongh, Phys. Rev. B **61**, 4699 (2000).
[42] P. A. Cox, *Transition Metal Oxides* (Oxford University Press, Oxford, 1992).
[43] *Ab initio* calculations of the defect states at (rutile) TiO_2 surfaces show that the intra-band-gap states due to potassium ion adsorption [J. Muscat and N. M. Harrison and G. Thornton, Phys. Rev. B **59**, 15 457 (1999)] are similar to those due to oxygen deficiency [W. C. Mackrodt, E. A. Simson and N. M. Harrison, Surf. Sci. **384**, 192 (1997)].
[44] S. Sodergren (private communication).
[45] L. A. Lyon and J. T. Hupp, J. Phys. Chem. B **103**, 4623 (1999).
[46] G. Boschloo and D. Fitzmaurice, J. Phys. Chem. B **103**, 7860 (1999).
[47] G. Pfister and H. Scher, Phys. Rev. B **15**, 2062 (1977).
[48] The relationship between stretched exponential relaxation and the mechanism of charge transport has been discussed, for instance, by I. Mihalcescu, J. C. Vial, and R. Romestain, Phys. Rev. Lett. **80**, 3392 (1998) for photoluminescence of porous silicon; and by U. Even, K. Rademann, J. Jortner, N. Manor, and R. Reisfeld, *ibid.* **52**, 2164 (1984) for photoluminescence of dyes on fractal porous glasses.
[49] A. C. Fisher, L. M. Peter, E. A. Ponomarev, A. B. Walker, and K. G. U. Wijayantha, J. Phys. Chem. B **104**, 949 (2000).
[50] Here we assume that the recombination reaction is first order in n. A higher-order reaction would lead to an even lower sensitivity of n to G than $n \propto G^{\alpha}$.